Schweizerischer Erdbebendienst
Service Sismologique Suisse
Servizio Sismico Svizzero
Swiss Seismological Service

ETH zürich

SITE CHARACTERIZATION REPORT

SCHAT: Châtillon (FR) - Ecole

Manuel Hobiger, Vincent Perron, Afifa Imtiaz, Donat Fäh

Last Modification: 07/07/2020

Schweizerischer Erdbebendienst (SED)
Service Sismologique Suisse
Servizio Sismico Svizzero
Servizi da Terratrembels Svizzer

ETH Zürich
Sonneggstrasse 5
8092 Zürich
Schweiz
manuel.hobiger@sed.ethz.ch

Contents

1 Introduction **5**

2 Geological setting **6**

3 Site characterization measurements **7**
3.1 Data set 7
3.2 H/V and RayDec ellipticity curves 8
3.3 Polarization analysis 8
3.4 3-component high-resolution FK 10
3.5 WaveDec 12
3.6 SPAC 13
3.7 Summary 15

4 Data inversion **17**
4.1 Inversion targets 17
4.2 Inversion parameterization 18
4.3 Inversion results 18
4.4 Overview of the inversion result 25
4.5 Site amplification 26
4.6 Quarter-wavelength representation 27

5 Conclusion **28**

References **29**

Summary

The free-field strong-motion station SCHAT was built in Châtillon (FR) next to the building that houses the administration and the school. We performed a passive seismic array measurement to characterize the soil underneath the station.
The near-surface soil structure is variable in the area, as the dominant H/V peak varies between 4.3 and 14.1 Hz across the array. The array measurements were analyzed with different techniques, namely 3-component HRFK, WaveDec and SPAC. All techniques gave similar dispersion curves. The dispersion curves for the fundamental modes of both Love and Rayleigh waves could be retrieved from around 2.6 to 18.0 Hz and 2.5 to 17.2 Hz, respectively.
The joint inversion of Love and Rayleigh wave dispersion curves and the Rayleigh wave ellipticity angle shows that the structure can be described by a first layer with shear-wave velocity of around 130 m/s and thickness of about 4.0 m, followed by a second layer down to about 16.5 m with a velocity of about 415 m/s and a third main layer with a velocity of around 850 m/s down to about 54 m depth, where the velocity increases to over 1500 m/s. The V_{S30} of the best models is about 394 m/s, corresponding to soil class B in EC8 and C in SIA261.

1 Introduction

In the framework of the second phase of the Swiss Strong Motion Network (SSMNet) renewal project, a new station was planned in Châtillon (FR). The site selection resulted in the building housing the school and the public administration as the best site in the area. The new station, called SCHAT, went operational on 14 November 2017. The location of the station is shown in Fig. 1.

Figure 1: Map showing the location of station SCHAT in Châtillon.

2 Geological setting

A geological map of the surroundings of station SCHAT is shown in Fig. 2. The station is located in a complex geological environment consisting of moraine and clay deposits. According to the map, most stations of the passive array measurement were located on moraine. The station is located around 300 m northeast of the La Lance fault, an active fault with a length of over 15 km stretching from the northwestern shore of Lake Neuchâtel to an end point south of Payerne. This fault is the source of an increased seismicity in the area over the last decades. One target of the station installation is to better locate earthquakes on this fault.

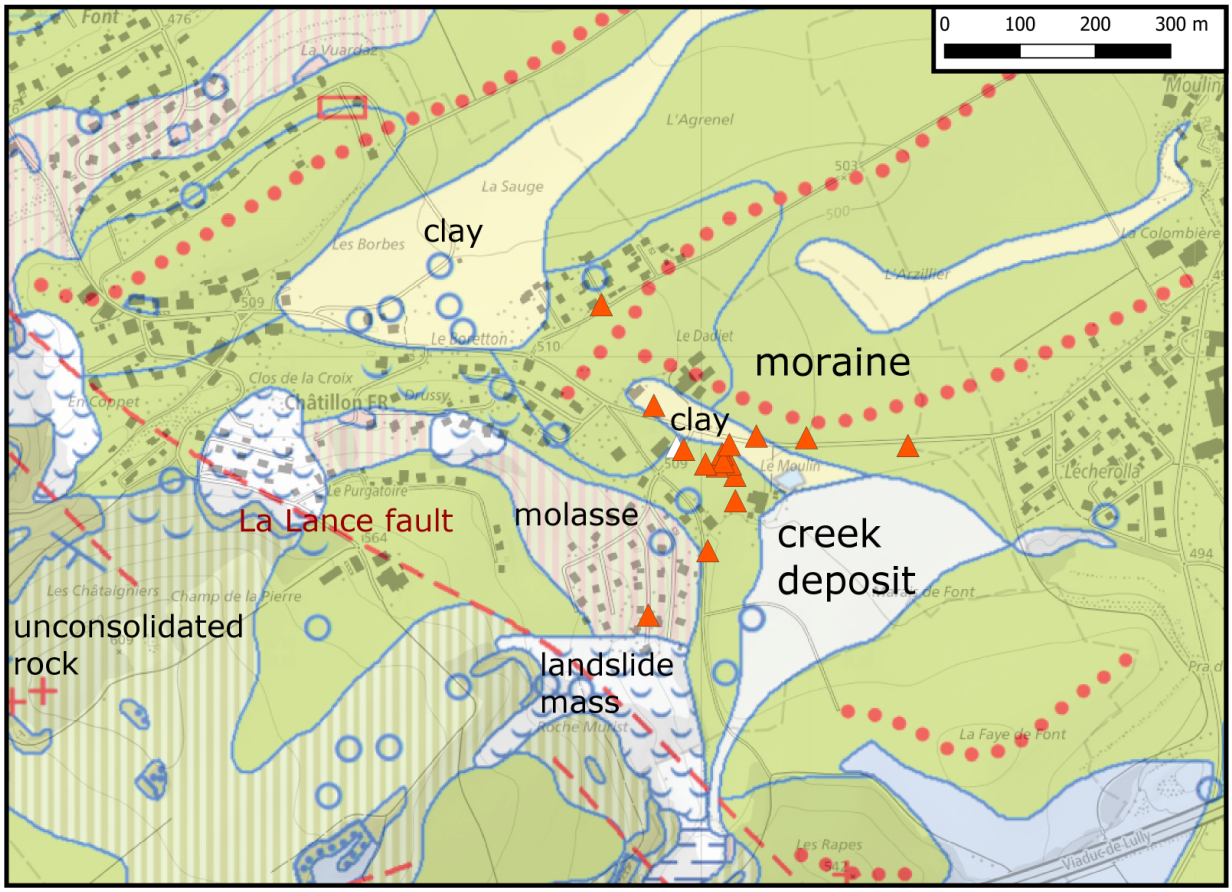

Figure 2: Geological map of the area around station SCHAT. According to the geological atlas, station SCHAT lies on moraine. ©2020 swisstopo (JD100042)

3 Site characterization measurements

3.1 Data set

In order to characterize the local underground structure around station SCHAT, a passive seismic array measurement was carried out on 16 October 2019. The layout of the seismic measurements is shown in Fig. 3.
A single array measurement was performed. The array consisted of 16 stations. It was planned to consist of five rings of three stations each around a central station, CHAT64. Station CHAT54 on the third ring was located close to the permanent station SCHAT. The final minimum and maximum inter-station distances in the array were 9.8 m and 447.9 m, respectively. The names of the stations of the array are composed of "CHAT" followed by a two-digit number (42 to 49, 52 to 55, 63 to 65, 69). The seismic stations consisted of Lennartz 3C 5 s sensors connected to Centaur digitizers. A total of 12 digitizers were used. Twelve sensors were connected to the A channels of the digitizers and another four sensors were connected to B channels. The total recording time was 154 minutes.
The station locations have been measured by a differential GPS system (Leica Viva GS10) which was set up to measure with a precision better than 5 cm. This precision was achieved for all stations. The array stations have been reoriented towards a common north by cross-correlating the respective signals with the horizontal component signals of CHAT64 in the frequency range from 0.3 to 1.0 Hz. Misorientations between $-6.48°$ and $5.42°$ were found.
Next to station CHAT64, and therefore close to the permanent station, a rotational sensor was deployed during the measurement for a test (see photo on the front page). These data are not part of this report.

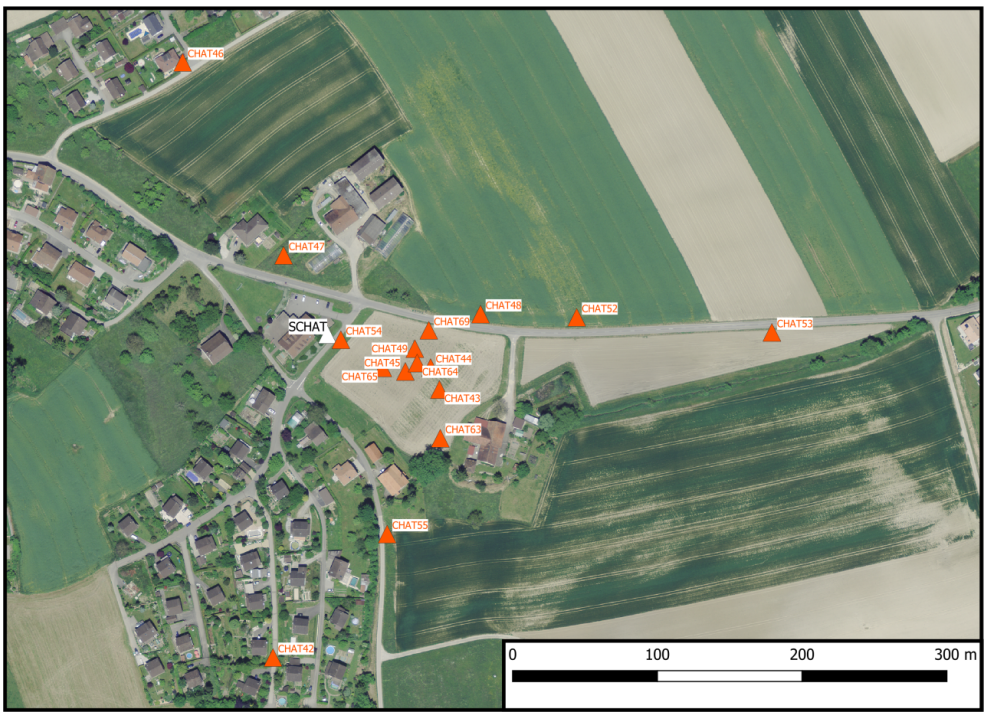

Figure 3: Layout of the array measurement around station SCHAT. ©2020 swisstopo (JD100042)

3.2 H/V and RayDec ellipticity curves

Figure 4 shows the H/V curves determined with the time-frequency analysis method (Fäh et al., 2009) for all stations of the passive array. The curves are similar for all stations below 2.5 Hz and show a wide, but not very pronounced peak at around 0.5 Hz. Above 2.5 Hz, the curves show a large variability with peak frequencies between 4.3 and 14.1 Hz. An overview map of these peak frequencies is also given in Fig. 4. Especially in the center of the array, the peak frequencies are systematically higher, with the station closest to the permanent station showing the highest value. This feature is probably caused by a smaller thickness of the superficial structure and might be linked with the clay structure indicated in Fig. 2.
The RayDec technique (Hobiger et al., 2009) is supposed to eliminate the contributions of other wave types than Rayleigh waves and give a better estimate of the ellipticity than the classical H/V technique. The RayDec ellipticity curves for all stations of the array measurements are also shown in Fig. 4 and are similar to the H/V curves. All curves show a trough around 3.5 Hz, which seems to be related with an anthropogenic source. Station CHAT64, the central station of the array, seems to be representative for most array stations and will be used later for the inversion.

3.3 Polarization analysis

The polarization analysis was performed according to Burjánek et al. (2010) and Burjánek et al. (2012). The results for all stations of the array are similar. Only the results for CHAT64, the station in the array center, are shown here.
There is no preferential linear particle polarization visible and we do not see indications for 2-dimensional polarization effects.

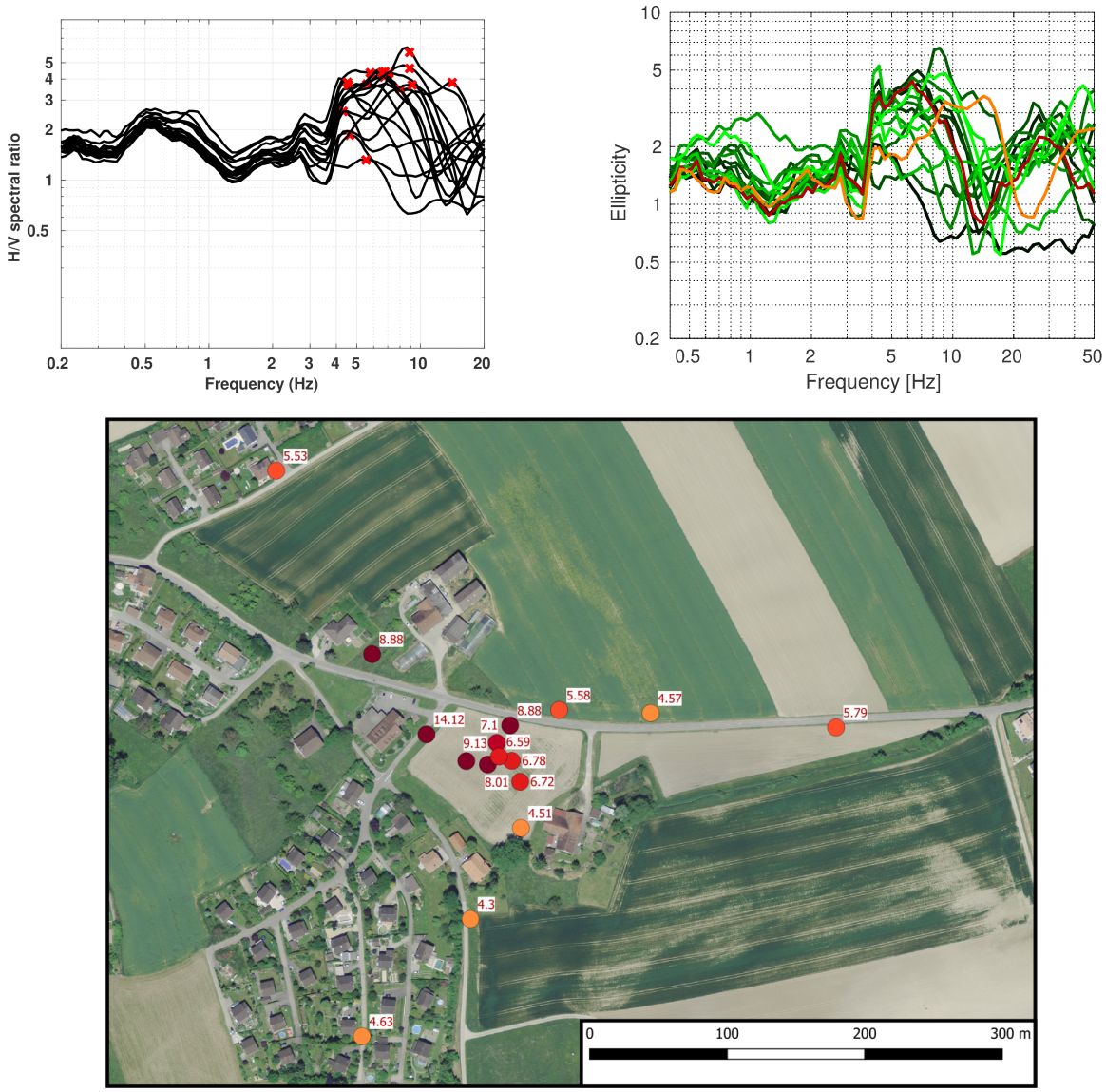

Figure 4: Top left: Overview of the H/V measurements for the different stations of the array measurement. Top right: RayDec ellipticities for all measurement stations. The red curve corresponds to CHAT64, the central station of the array. The orange curve corresponds to CHAT54, the station located closest of the permanent station SCHAT. Bottom: Overview map with the picked H/V peak frequencies. ©2020 swisstopo (JD100042)

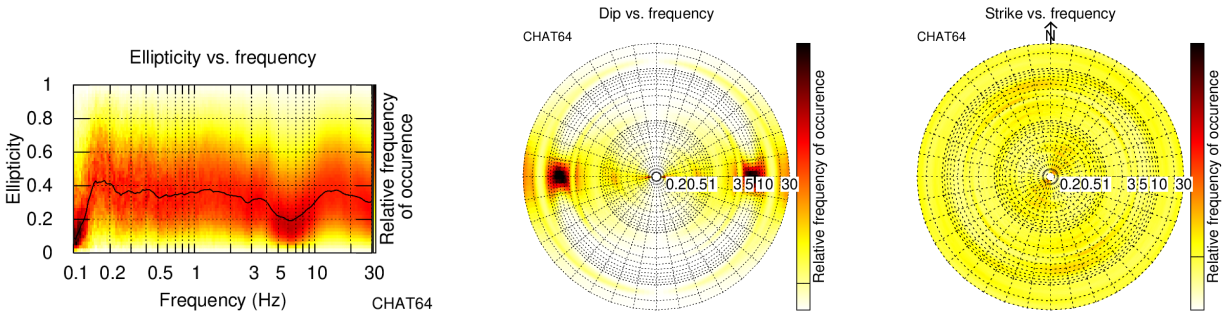

Figure 5: Polarization analysis of station CHAT64.

3.4 3-component high-resolution FK

The results of the 3-component high-resolution FK analysis (Poggi and Fäh, 2010) are shown in Fig. 6. On the transverse component, corresponding to Love waves, we can clearly identify a continuous dispersion curve from 2.6 up to 18.0 Hz, spanning the entire accessible frequency range of the array.
On the vertical component, corresponding to Rayleigh waves, the dispersion curve picking is more complicated. In total, four different dispersion curve segments were picked, but the mode attribution is not clear. The first segment (2.5 - 3.3 Hz) and the second segment (3.6 - 12.2 Hz) do not seem to correspond to the same mode. The third segment (8.8 - 10.6 Hz) is also visible on the radial component and might actually be mispicked. The fourth segment (11.9 - 17.2 Hz) doesn't fit well with the second segment, but might be the same mode as the first segment. On the radial component, also related with Rayleigh waves, a single continuous dispersion curve can be identified between 2.8 and 15.7 Hz.
The corresponding ellipticity curves of these modes are mostly flat and will be compared with the single-station ellipticity curves at a later stage.

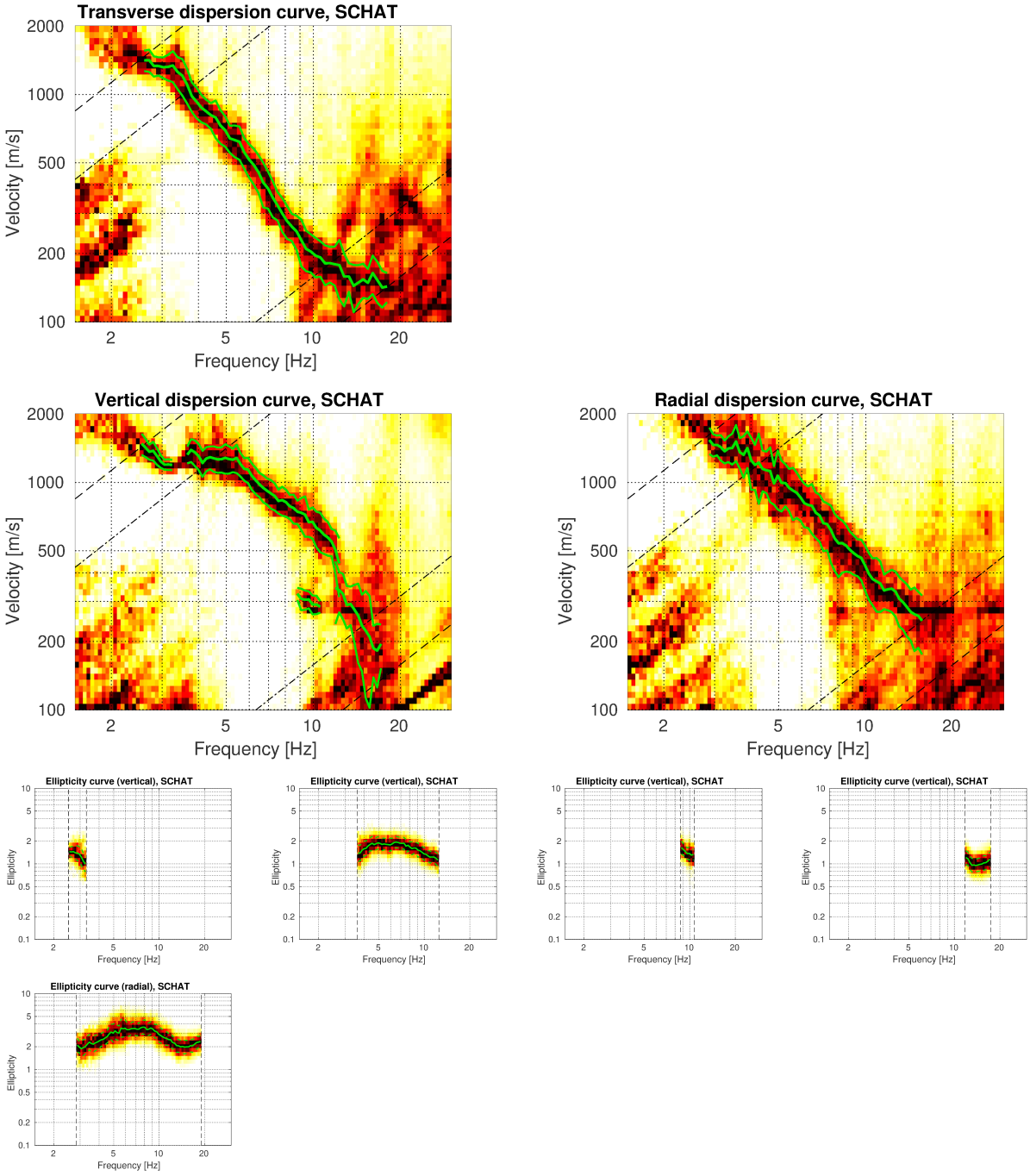

Figure 6: Dispersion and ellipticity curves obtained with the 3-component HRFK algorithm (Poggi and Fäh, 2010). In the top two lines, the dispersion curves for the transverse, vertical and radial components are shown, and in the two bottom lines the ellipticity curves corresponding to the dispersion curve segments picked on the vertical and radial components. The dashed and dotted black lines are the array resolution limits. The solid green lines are picked from the data, where the central line indicates the best values and the two outer lines the standard deviation.

3.5 WaveDec

The results of the WaveDec (Maranò et al., 2012) processing are shown in Fig. 7. This technique estimates the properties of single or multiple waves simultaneously with a maximum likelihood approach. In order to improve the results, the parameter γ, which modifies the sharpness of the wave property estimation, has been tuned. Here, a value of $\gamma = 0.2$ was used, corresponding to a predominantly maximum likelihood estimation. The Love wave dispersion curve is well retrieved and picked between 2.6 and 12.4 Hz. The Rayleigh wave dispersion curve is less clear, but can be picked between 2.8 and 14.9 Hz. The ellipticity angles for the picked Rayleigh wave dispersion curves are negative (retrograde particle motion) below around 4 Hz and positive (prograde particle motion) above, but the actual frequency of the change is not clear. Above this frequency, the ellipticity angle is close to 90° up to over 10 Hz.

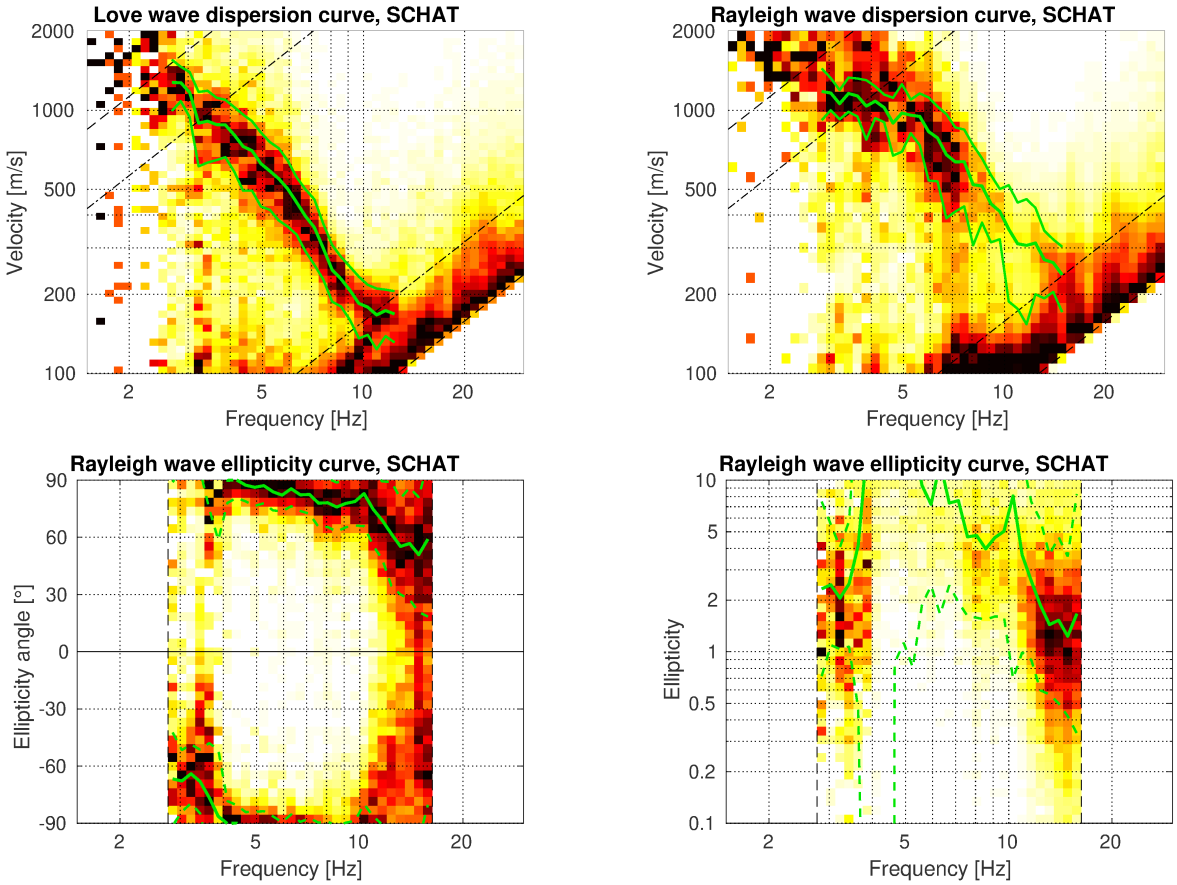

Figure 7: Top: Love (left) and Rayleigh (right) wave dispersion curves obtained with the WaveDec technique (Maranò et al., 2012). The dashed lines indicate the theoretical array resolution limits. Bottom left: Rayleigh wave ellipticity angle curve for the picked dispersion curve. Bottom right: Rayleigh wave ellipticity curve, i.e. the absolute value of the tangent of the ellipticity angle curve shown on the left.

3.6 SPAC

The SPAC (Aki, 1957) curves of the vertical components have been calculated using the M-SPAC (Bettig et al., 2001) technique implemented in geopsy. Rings with different radius ranges had been defined previously and for all station pairs with distance inside this radius range, the cross-correlation was calculated over a wide frequency range. These cross-correlation curves are averaged for all station pairs of the respective ring and give the SPAC curves. The rings are defined in such a way that at least three station pairs contribute and that their connecting vectors have a good directional coverage.
The SPAC curves for all defined rings are shown in Fig. 8. The black points indicate the data values which contributed to the final dispersion curve estimation, which was made with the function `spac2disp` of the geopsy package. These resulting dispersion curves are shown in Fig. 9.
The calculated SPAC curves have the shape of the theoretical Bessel functions. The retrieved Rayleigh wave dispersion curve ranges from 3.2 to 13.8 Hz.

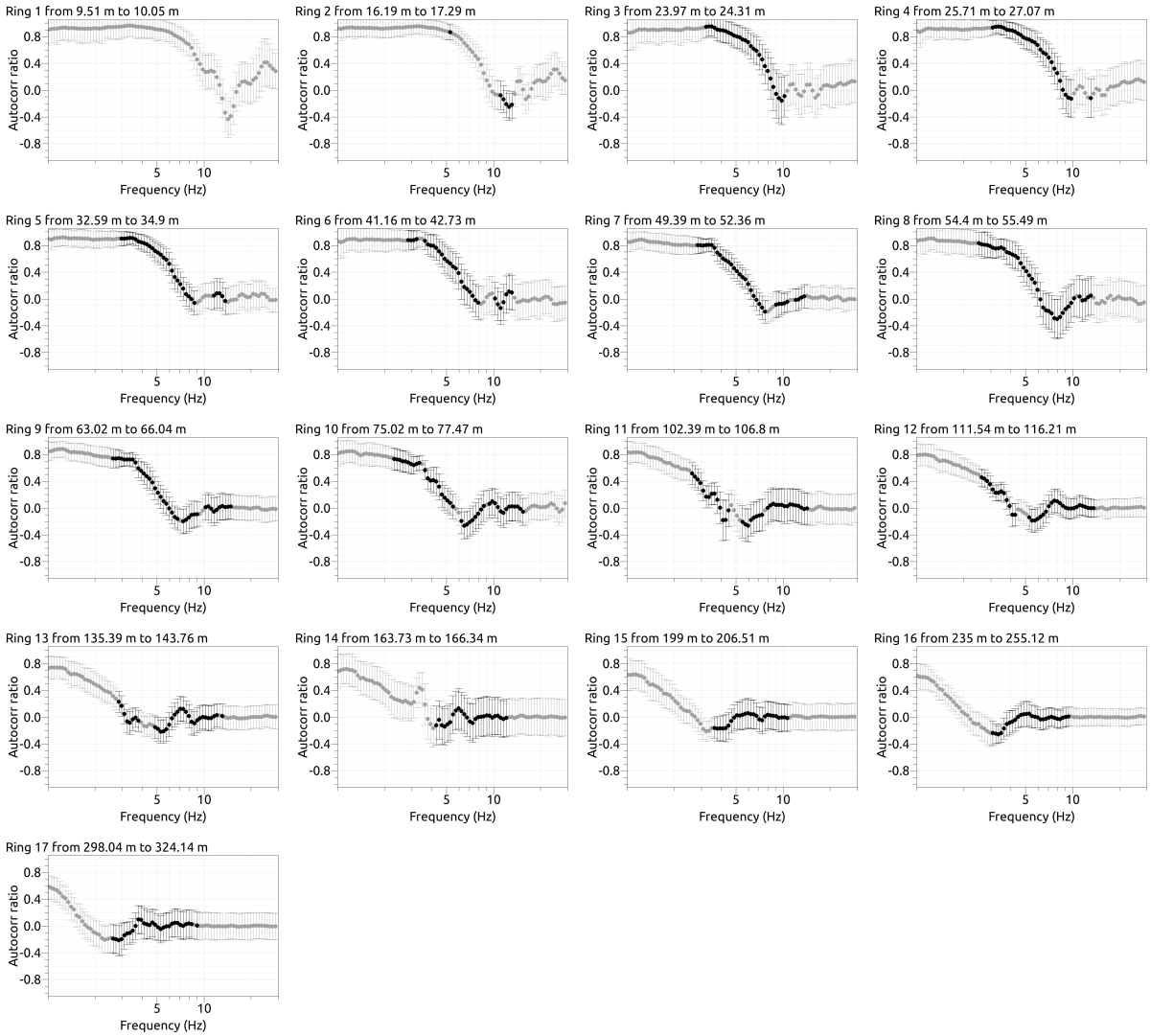

Figure 8: SPAC curves for all radius ranges. The black data points contributed to the dispersion curve estimation.

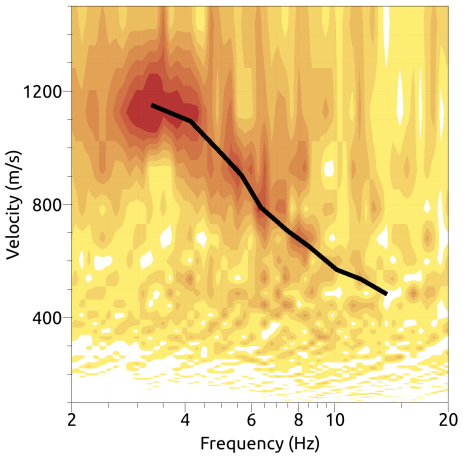

Figure 9: Resulting Rayleigh wave velocities for the curves in Fig. 8.

3.7 Summary

Fig. 10 gives an overview of the dispersion and ellipticity curves determined by the different methods.
For Love waves, the HRFK and WaveDec results are in good overall agreement, with major differences only below 4 Hz.
For the Rayleigh waves, there are major differences between the different methods and components, but they can be interpreted together. The fundamental model seems to consist of the first 3C-HRFK segment picked on the vertical component, below 3.5 Hz. It then follows the WaveDec curve, which is joined at around 5 Hz by the radial components 3C-HRFK curve and at around 12 Hz by the fourth picked vertical 3C-HRFK segment. In this interpretation, the second segment picked on the vertical 3C-HRFK plot corresponds to the first harmonic mode. It is however unclear if the part of this curve below 5.5 Hz also belongs to this mode or is a mixture between the fundamental and first higher modes. The SPAC curve, in any case, is an apparent mode with a mixture of the different curves here.
The ellipticity curves retrieved using the different methods show some variability. The single-station ellipticity curve determined with RayDec at the array center (CHAT64) is in better agreement with the array curves than the one close to the permanent station (CHAT54). The WaveDec curve shows a singularity between 4 and 5 Hz, but seems in overall qualitative agreement with the other curves. A trough at higher frequencies is not visible, but can be expected around 15 Hz from the RayDec curve. The inversion will show if it is realistic to have a high ellipticity value over such a wide frequency range.
The last plot shows the ellipticity angle. The RayDec curve was transformed to ellipticity angle by using the arctan function. As we cannot distinguish between prograde and retrograde particle motion with a single-station method, we account for both possibilities and the RayDec (and HRFK) curves are represented twice, once for each sense of rotation.

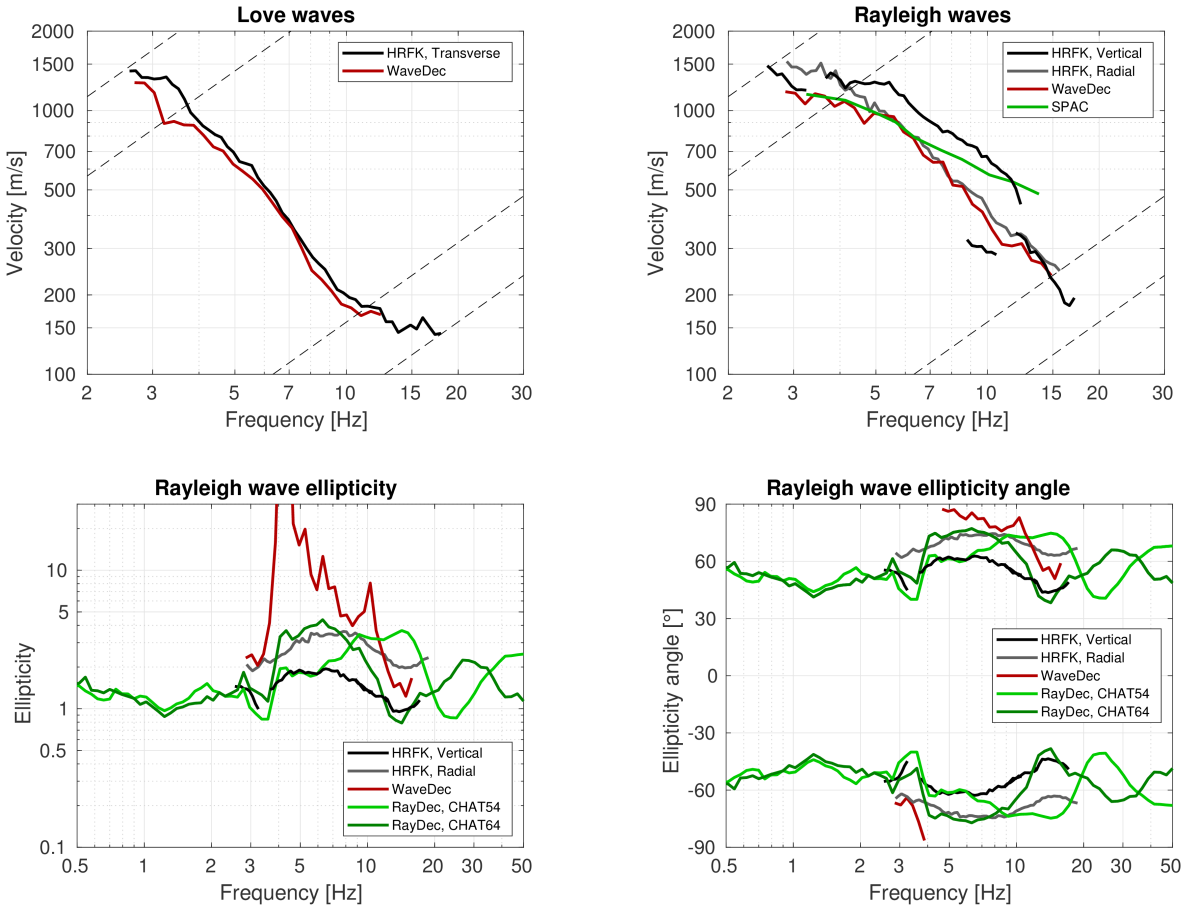

Figure 10: Overview of the Love and Rayleigh wave dispersion curves as well as the ellipticity and ellipticity angle curves for both arrays. The dashed lines indicate the theoretical resolution limits of the array.

4 Data inversion

4.1 Inversion targets

We performed inversions using the fundamental Love wave dispersion curve, the fundamental and first higher Rayleigh wave dispersion curve, and the Rayleigh wave ellipticity angle as inversion targets. The details of the inversion targets are indicated in Table 1 and the corresponding curves are shown in Fig. 11.
For the Love wave dispersion curve, the HRFK curve was used. For the fundamental mode Rayleigh wave curve, parts of HRFK for the vertical and radial components and WaveDec were used. A part of the vertical HRFK curves was used for the first higher Rayleigh wave mode.
For the ellipticity angle, we tested the use of the RayDec curve of CHAT 54, but without good fit. Therefore, the WaveDec measurement was used, with retrograde particle motion below 4.5 Hz and prograde one above.

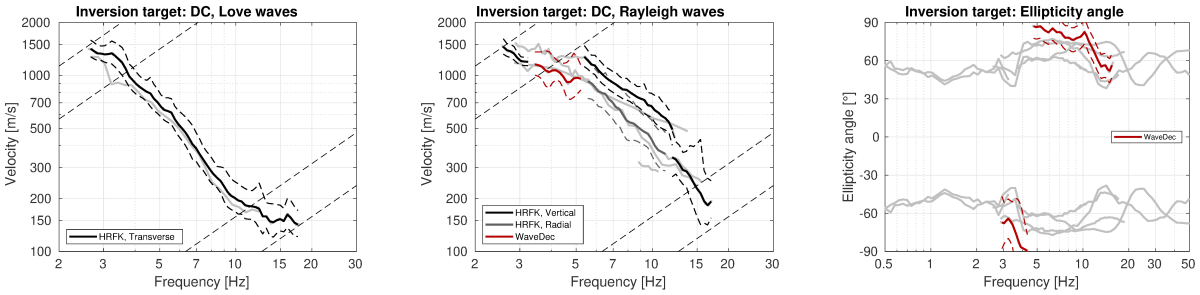

Figure 11: Overview of the dispersion and ellipticity angle curves used as targets for the different inversions.

Table 1: List of the different data curves used as target in the inversions.

Method	Wave type	Mode	Curve type	Frequency range [Hz]
HRFK (T)	Love	fundamental	dispersion	2.66 - 17.59
HRFK (V)	Rayleigh	fundamental	dispersion	2.58 - 3.23
WaveDec	Rayleigh	fundamental	dispersion	3.44 - 5.22
HRFK (R)	Rayleigh	fundamental	dispersion	5.56 - 11.24
HRFK (V)	Rayleigh	fundamental	dispersion	11.98 - 17.03
HRFK (V)	Rayleigh	first higher	dispersion	5.38 - 11.98
WaveDec	Rayleigh	fundamental	ellipticity angle	2.93 - 4.31
WaveDec	Rayleigh	fundamental	ellipticity angle	4.74 - 15.48

4.2 Inversion parameterization

Six different parameterizations were used for the inversions. The first five had free values of the depths and velocities of the different layers, ranging from four to eight layers (including half-space). The last parameterization had fixed layer depths and consisted of 20 layers in total, using reasonable depths for the interfaces. The P-wave velocities were allowed to vary up to 5000 m/s. The S-wave velocities were allowed to range from 50 to 3500 m/s. The deepest layers were parameterized to range to a depth of 200 m maximum. The density was fixed to 2 300 kg/m^3 for the lowest layer, to 1 900 kg/m^3 for the superficial layer (or the first three layers in the fixed-layer case) and to 2 100 kg/m^3 for all other layers. No low-velocity zones were allowed.

4.3 Inversion results

For each parameterization, 20 different runs were performed, but only the one giving the best minimum misfit was kept. In Table 2, the obtained minimum misfit values for these inversions are shown. Each inversion run produced at least around 150 000 total models in order to assure a good convergence of the solution, except for the 8-layer and the fixed-depth inversions, where about 200 000 models were generated. The results of the inversions SCHAT4l to SCHATfix are shown in Figs 12 - 17.
The different inversions yield similar misfit values and fit the data in a comparable way. The fixed-depth inversion shows slightly higher misfits, probably because the interface depths were not optimal.

Table 2: List of inversions

Inversion	Number of layers	Number of models	Minimum misfit
SCHAT4l	4	149 999	0.293
SCHAT5l	5	150 051	0.278
SCHAT6l	6	150 021	0.278
SCHAT7l	7	150 006	0.279
SCHAT8l	8	200 043	0.280
SCHATfix	20	200 016	0.319

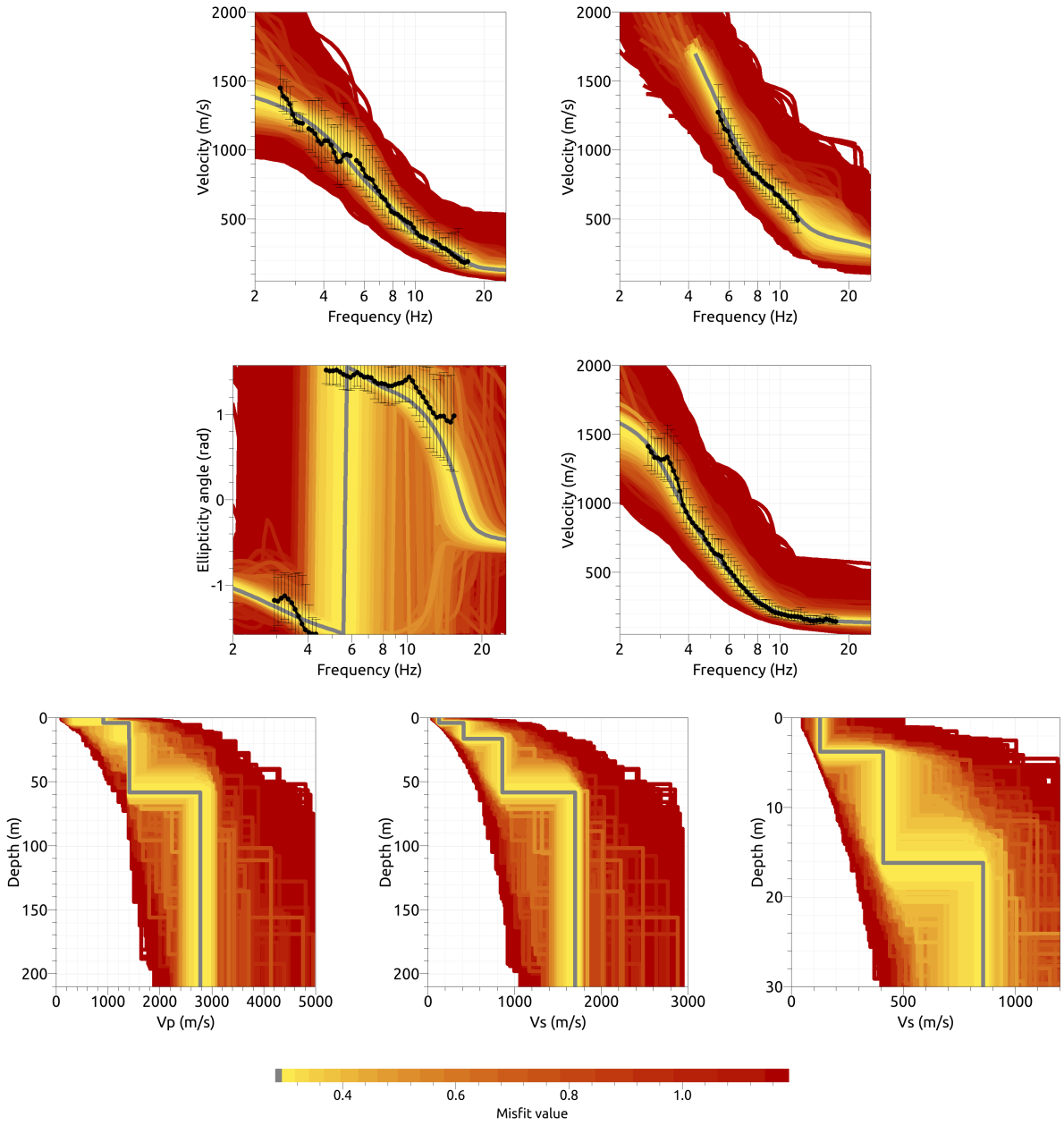

Figure 12: Inversion SCHAT4l. Top line: Dispersion curves for the fundamental (left) and first higher (right) mode of Rayleigh waves. Center line: Ellipticity angle for the fundamental Rayleigh wave mode (left) and dispersion curve for the fundamental Love wave mode (right). Bottom line: P-wave velocity profiles (left), S-wave velocity profiles (center and zoom on the upper 30 m on the right). All generated models are plotted on top of each other in the color corresponding to the respective misfit value. The black dots indicate the data points used for the inversion, the gray line indicates the best-fitting model.

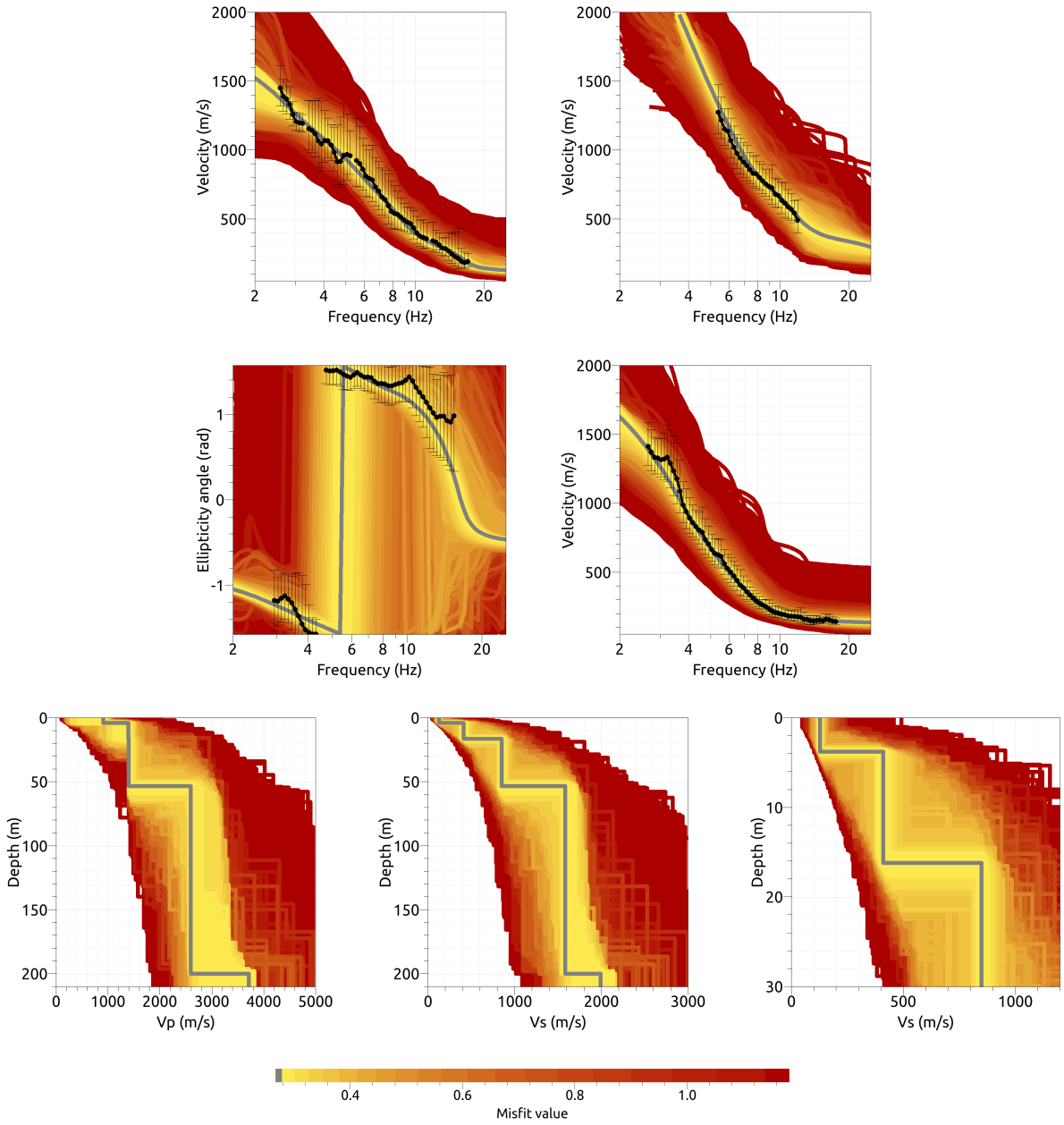

Figure 13: Inversion SCHAT5l. Top line: Dispersion curves for the fundamental (left) and first higher (right) mode of Rayleigh waves. Center line: Ellipticity angle for the fundamental Rayleigh wave mode (left) and dispersion curve for the fundamental Love wave mode (right). Bottom line: P-wave velocity profiles (left), S-wave velocity profiles (center and zoom on the upper 30 m on the right). All generated models are plotted on top of each other in the color corresponding to the respective misfit value. The black dots indicate the data points used for the inversion, the gray line indicates the best-fitting model.

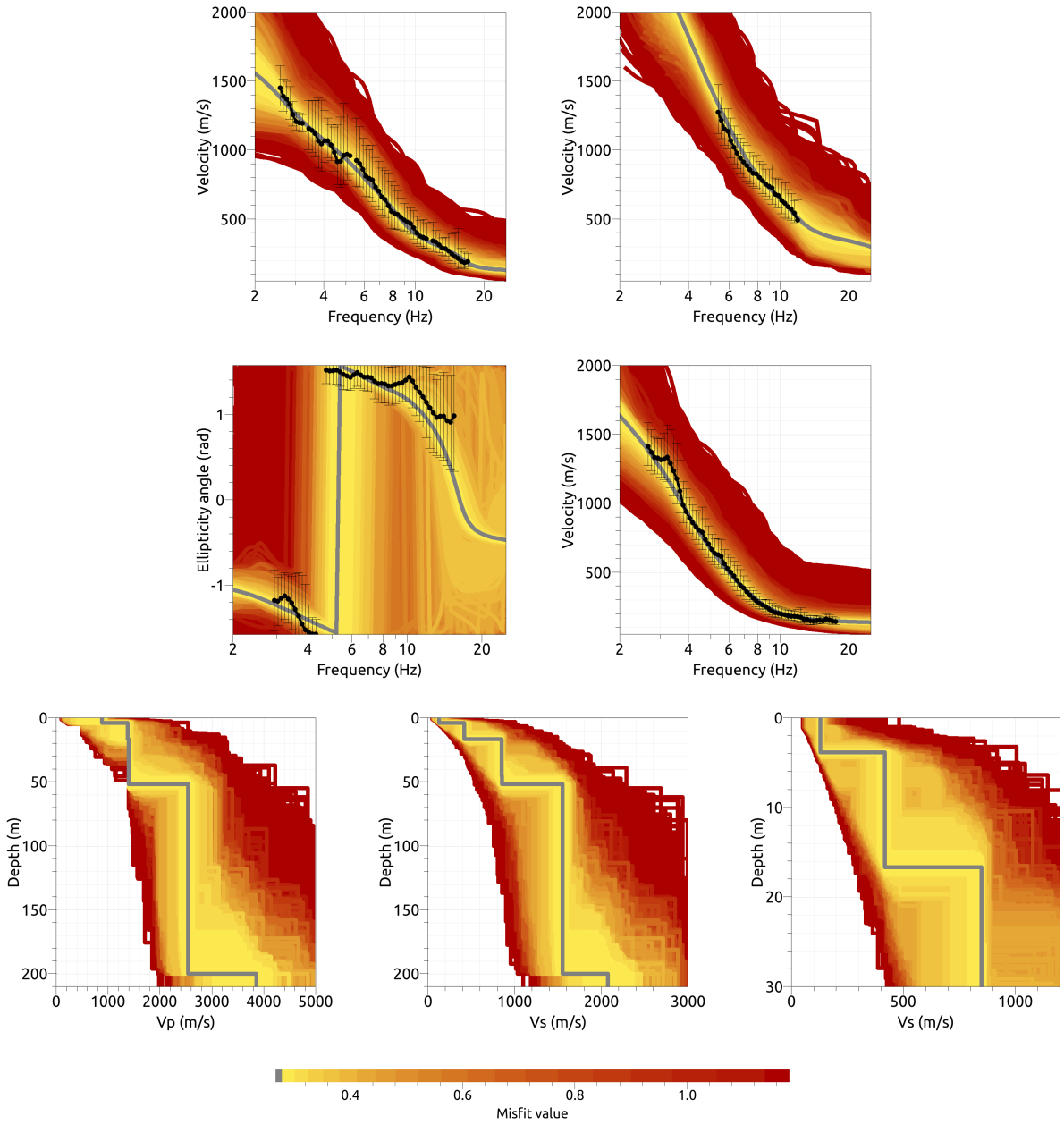

Figure 14: Inversion SCHAT6l. Top line: Dispersion curves for the fundamental (left) and first higher (right) mode of Rayleigh waves. Center line: Ellipticity angle for the fundamental Rayleigh wave mode (left) and dispersion curve for the fundamental Love wave mode (right). Bottom line: P-wave velocity profiles (left), S-wave velocity profiles (center and zoom on the upper 30 m on the right). All generated models are plotted on top of each other in the color corresponding to the respective misfit value. The black dots indicate the data points used for the inversion, the gray line indicates the best-fitting model.

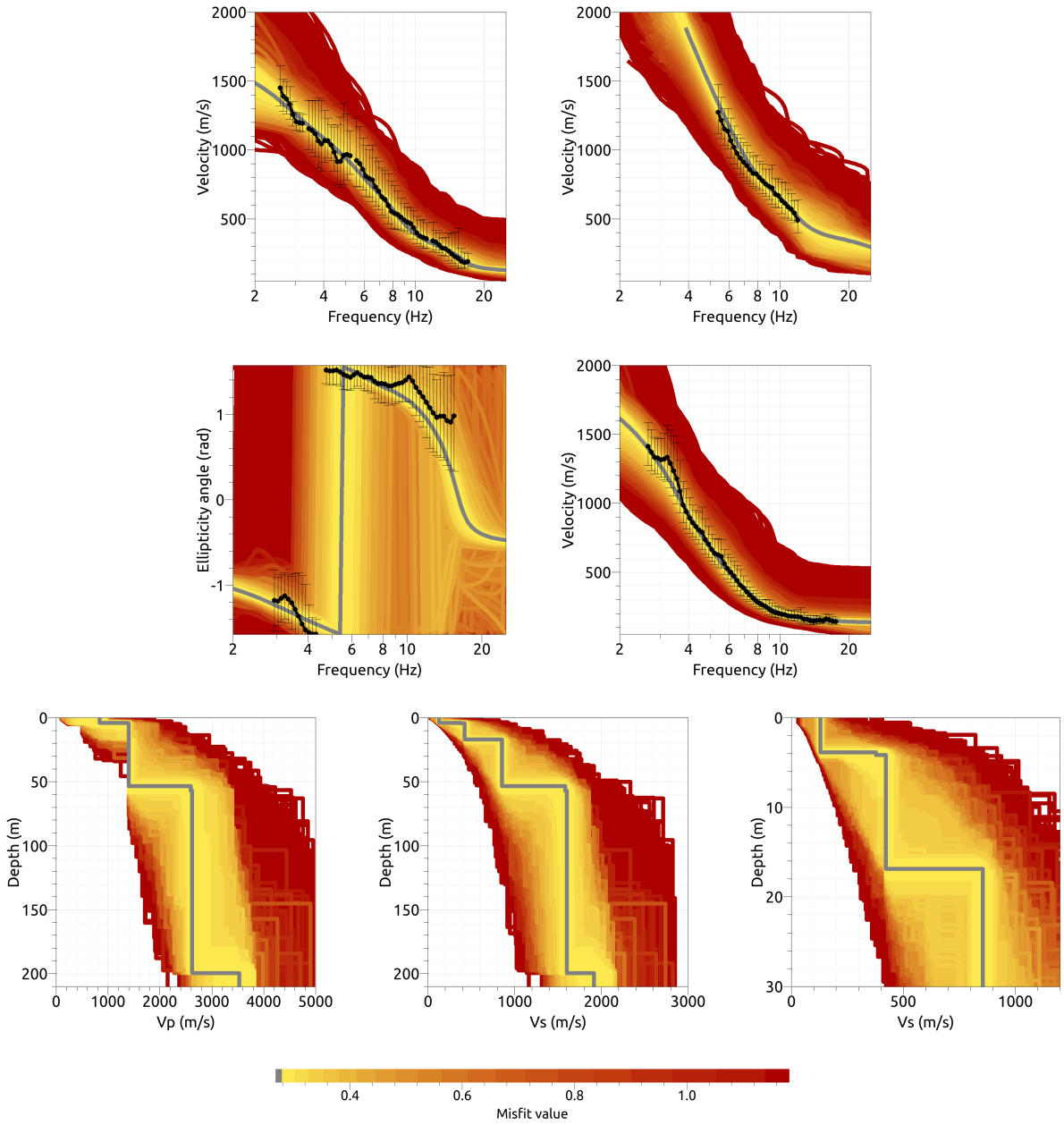

Figure 15: Inversion SCHAT7l. Top line: Dispersion curves for the fundamental (left) and first higher (right) mode of Rayleigh waves. Center line: Ellipticity angle for the fundamental Rayleigh wave mode (left) and dispersion curve for the fundamental Love wave mode (right). Bottom line: P-wave velocity profiles (left), S-wave velocity profiles (center and zoom on the upper 30 m on the right). All generated models are plotted on top of each other in the color corresponding to the respective misfit value. The black dots indicate the data points used for the inversion, the gray line indicates the best-fitting model.

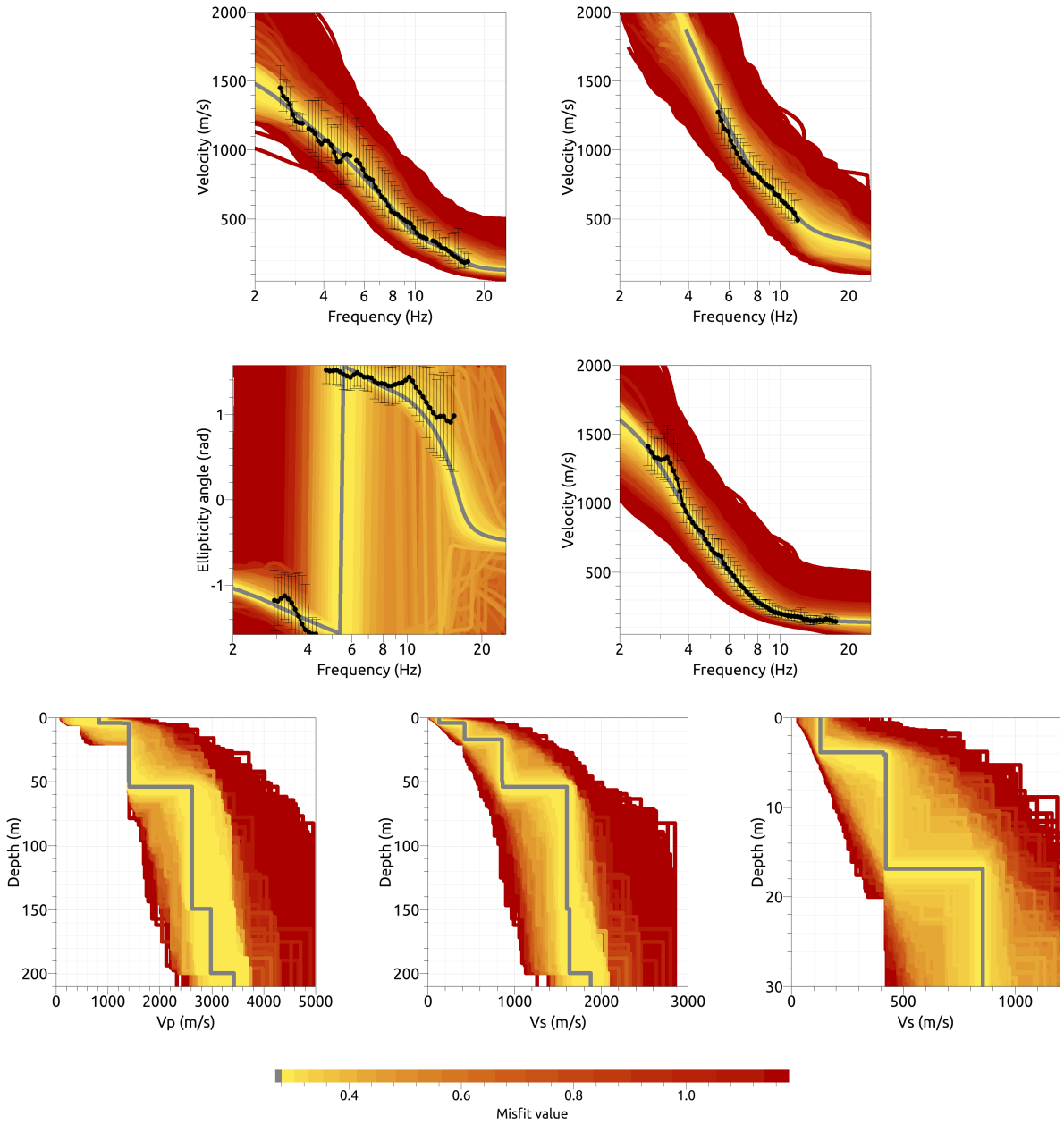

Figure 16: Inversion SCHAT8l. Top line: Dispersion curves for the fundamental (left) and first higher (right) mode of Rayleigh waves. Center line: Ellipticity angle for the fundamental Rayleigh wave mode (left) and dispersion curve for the fundamental Love wave mode (right). Bottom line: P-wave velocity profiles (left), S-wave velocity profiles (center and zoom on the upper 30 m on the right). All generated models are plotted on top of each other in the color corresponding to the respective misfit value. The black dots indicate the data points used for the inversion, the gray line indicates the best-fitting model.

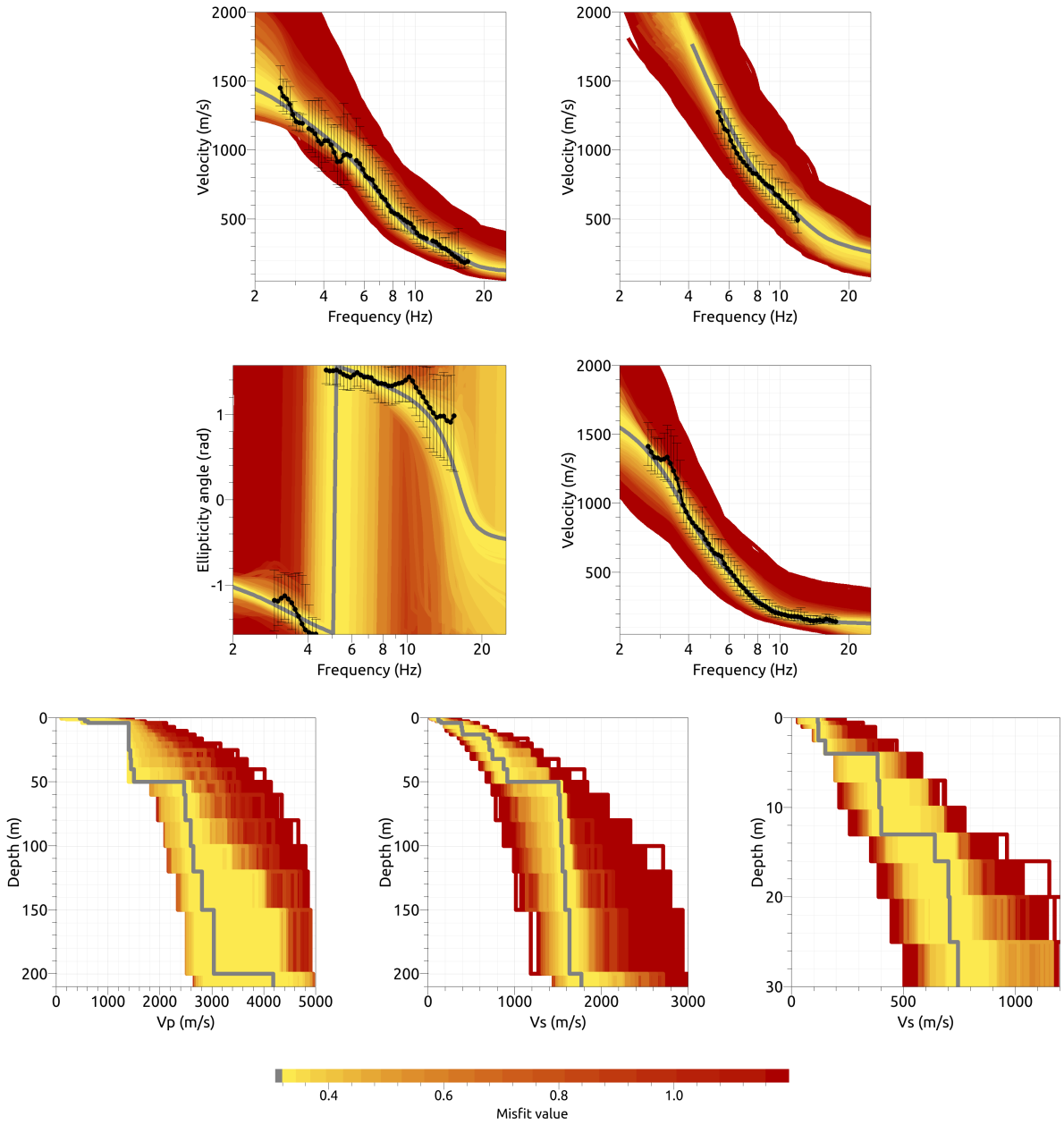

Figure 17: Inversion SCHATfix. Top line: Dispersion curves for the fundamental (left) and first higher (right) mode of Rayleigh waves. Center line: Ellipticity angle for the fundamental Rayleigh wave mode (left) and dispersion curve for the fundamental Love wave mode (right). Bottom line: P-wave velocity profiles (left), S-wave velocity profiles (center and zoom on the upper 30 m on the right). All generated models are plotted on top of each other in the color corresponding to the respective misfit value. The black dots indicate the data points used for the inversion, the gray line indicates the best-fitting model.

4.4 Overview of the inversion result

The best-fitting models of the inversions SCHAT4l-SCHATfix are shown in Fig. 18. All models show similar main features. The superficial layer with a thickness of about 3.7 to 4.0 m has a shear-wave velocity of about 130 m/s, followed by a layer with a velocity of 410 to 420 m/s down to about 16.1 to 16.8 m, where the velocity increases to around 850 m/s. Another interface is found at around 50 to 58 m depths with an increase of the velocity to over 1500 m/s. A final interface is found at 200 m depth with a small increase in velocity. As this depths was the limit of the inversion parameterization and deeper layers cannot be resolved with the used information, this interface is not well constrained.
All inversions are accepted as representative models for the underground structure. The V_{S30} value for these inversions ranges from 386.1 to 395.9 m/s (average value 394.2 $\pm$ 4.0 m/s). This corresponds to soil class B in EC8 and C in SIA261.

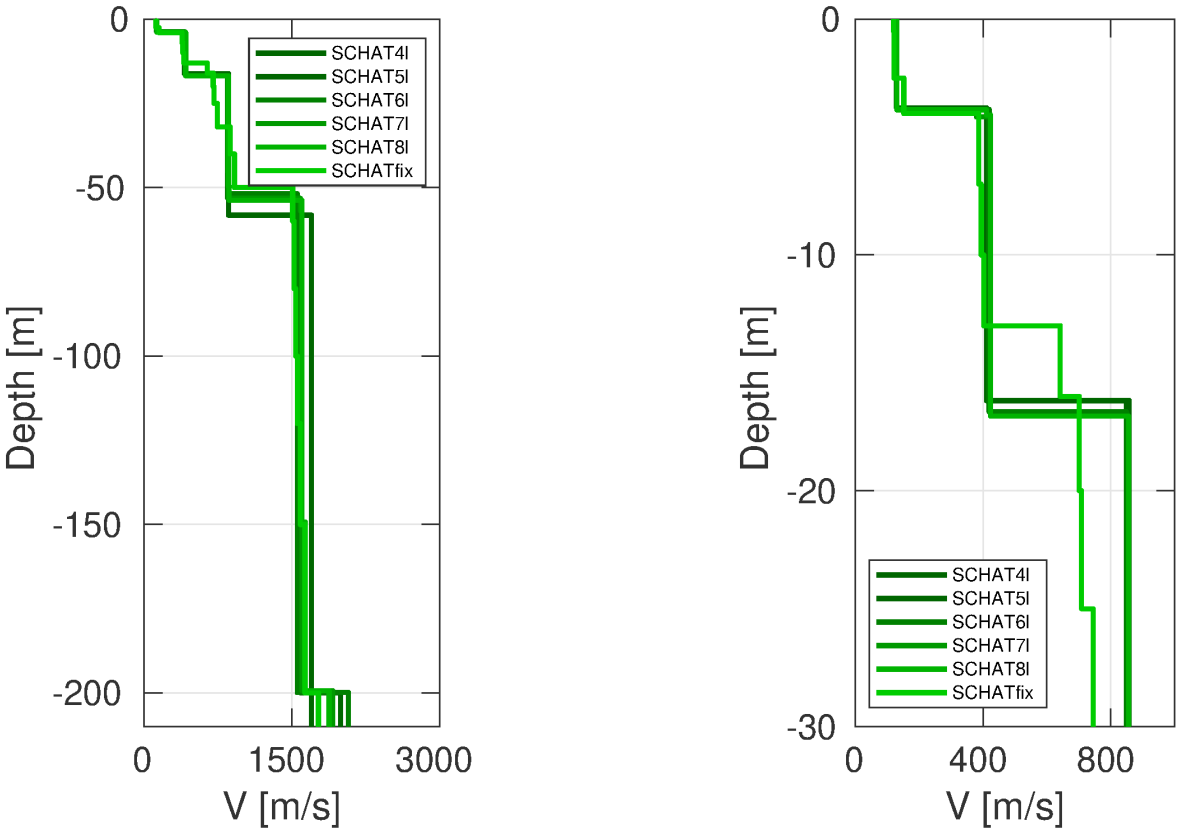

Figure 18: Overview of shear-wave velocity profiles of the best-fitting models of all inversions (left) and a zoom on the shallow part (right).

4.5 Site amplification

In Fig. 19, the theoretical amplification function for the best models resulting from the six selected inversions is compared with the empirical amplification. The empirical amplification for station SCHAT is based on 27 events so far. There is some qualitative, but not quantitative agreement. Below 2 Hz, where the profiles resulting from the inversion are not constrained, the empirical amplification is higher, with amplification values of up to 3. Between 2 and 13 Hz, the modeled amplification is higher and overestimates the empirical amplification by a factor of up to 2. It should be noted that the peak frequencies around 7 Hz and at 11 Hz are in good agreement.
From the H/V and ellipticity measurements, a difference between the array center and the station location was visible. These small-scale heterogeneities in the superficial layers may play a role here.

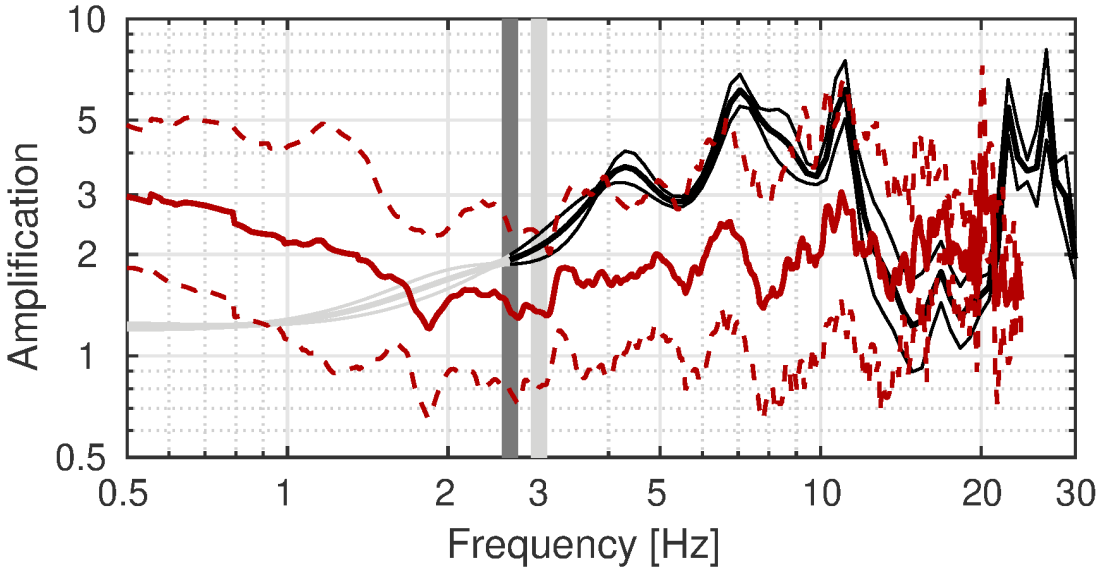

Figure 19: Comparison between the modeled amplification for the final set of best models of the different inversions (SCHAT4l-SCHATfix; in gray to black, with standard deviation) and the empirical amplification measured at station SCHAT (red, with standard deviation). The vertical light and dark grey bars correspond to the lowest frequency of the ellipticity and dispersion curves, respectively.

4.6 Quarter-wavelength representation

The quarter-wavelength velocity approach (Joyner et al., 1981) provides, for a given frequency, the average velocity at a depth corresponding to 1/4 of the wavelength of interest. It is useful to identify the frequency limits of the experimental data (the minimum frequency of the dispersion curve used in the inversion is 2.58 Hz, the minimum frequency used for the ellipticity inversion 2.93 Hz). The results using this proxy show that the dispersion curves constrain the profiles down to only about 45 m (Fig. 20). Moreover, the quarter wavelength impedance-contrast introduced by Poggi et al. (2012) is also displayed in the figure. It corresponds to the ratio between two quarter-wavelength average velocities, respectively from the top and the bottom part of the velocity profile, at a given frequency (Poggi et al., 2012). This curve shows a wide plateau between 3 and 10 Hz.

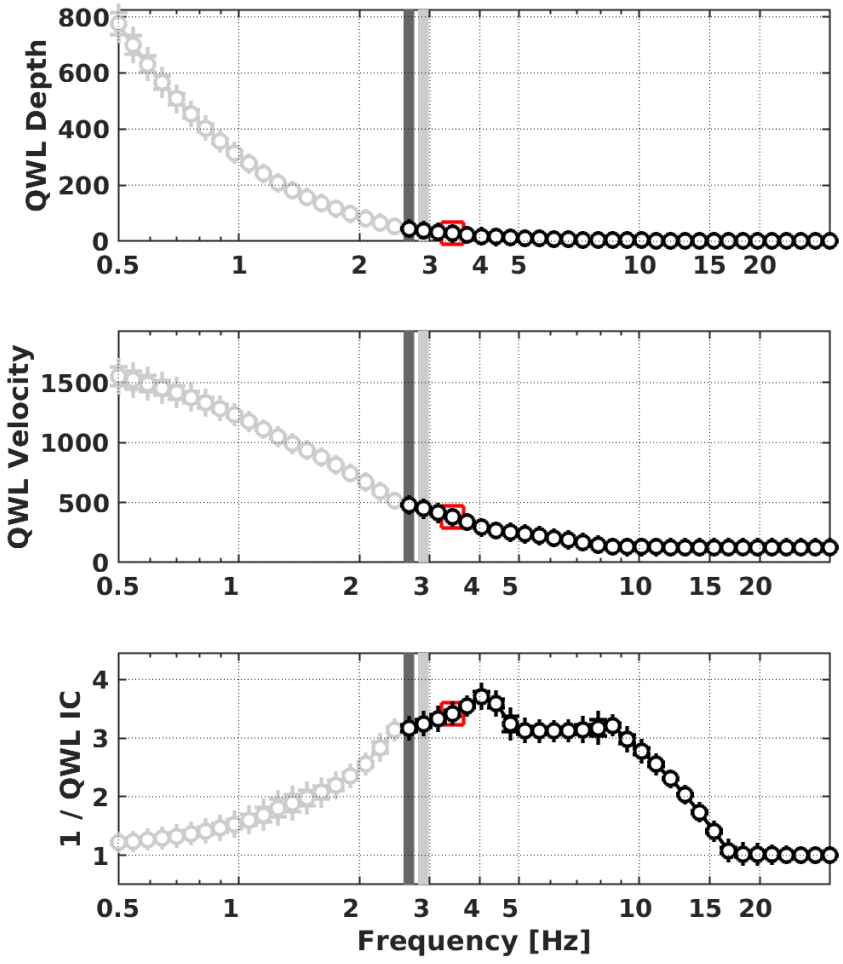

Figure 20: Quarter wavelength representation of the velocity profile for the best models of the inversions (top: depth, center: velocity, bottom: inverse of the impedance contrast). The black curves are constrained by the dispersion curves, the light grey curves are not constrained by the data. The red square corresponds to V_{S30}.

5 Conclusion

We performed a passive array measurement to characterize the soil underneath station SCHAT in Châtillon (FR), located on a complex geology consisting of moraine and clay deposits, in the vicinity of the La Lance fault.
The dispersion curves for Love and Rayleigh waves could be measured over a wide frequency range, from around 2.6 to 18.0 Hz for Love waves and from 2.5 to 17.2 Hz for Rayleigh waves. The ellipticity curves show a consistent low-frequency peak at around 0.5 Hz, which is not very pronounced, and a stronger peak of variable frequency ranging from 4.3 to 14.1 Hz.
The joint inversion of Love and Rayleigh wave dispersion curves and the Rayleigh wave ellipticity angle showed that the structure can be described by a first layer with shear-wave velocity of around 130 m/s and thickness of about 4.0 m, a second layer down to about 16.5 m with a velocity of about 415 m/s, followed by a third main layer with a velocity of around 850 m/s down to about 54 m depth, where the velocity increases to over 1500 m/s. The V_{S30} of the best models is about 394 m/s, corresponding to soil class B in EC8 and C in SIA261.

References

Aki, K. (1957). Space and time spectra of stationary stochastic waves, with special reference to microtremors. *Bull. Earthquake Res. Inst. Tokyo Univ.*, 35:415–456.

Bettig, B., Bard, P.-Y., Scherbaum, F., Riepl, J., Cotton, F., Cornou, C., and Hatzfeld, D. (2001). Analysis of dense array noise measurements using the modified spatial auto-correlation method (SPAC): application to the Grenoble area. *Boll. Geof. Teor. Appl.*, 42:281–304.

Burjánek, J., Gassner-Stamm, G., Poggi, V., Moore, J. R., and Fäh, D. (2010). Ambient vibration analysis of an unstable mountain slope. *Geophys. J. Int.*, 180:820–828.

Burjánek, J., Moore, J. R., Molina, F. X. Y., and Fäh, D. (2012). Instrumental evidence of normal mode rock slope vibration. *Geophys. J. Int.*, 188:559–569.

Fäh, D., Wathelet, M., Kristekova, M., Havenith, H., Endrun, B., Stamm, G., Poggi, V., Burjanek, J., and Cornou, C. (2009). Using ellipticity information for site characterisation. NERIES deliverable JRA4 D4, available at http://www.neries-eu.org.

Hobiger, M., Bard, P.-Y., Cornou, C., and Le Bihan, N. (2009). Single station determination of Rayleigh wave ellipticity by using the random decrement technique (RayDec). *Geophys. Res. Lett.*, 36.

Joyner, W. B., Warrick, R. E., and Fumal, T. E. (1981). The effect of Quaternary alluvium on strong ground motion in the Coyote Lake, California, earthquake of 1979. *Bull. Seismol. Soc. Am.*, 71(4):1333–1349.

Maranò, S., Reller, C., Loeliger, H.-A., and Fäh, D. (2012). Seismic waves estimation and wavefield decomposition: Application to ambient vibrations. *Geophys. J. Int.*, 191:175–188.

Poggi, V., Edwards, B., and Fäh, D. (2012). Characterizing the Vertical-to-Horizontal ratio of ground motion at soft-sediment sites. *Bull. Seismol. Soc. Am.*, 102(6):2741–2756.

Poggi, V. and Fäh, D. (2010). Estimating Rayleigh wave particle motion from three-component array analysis of ambient vibrations. *Geophys. J. Int.*, 180:251–267.